Atomic-scale investigation of graphene formation on 6*H*-SiC(0001)

N. P. Guisinger[a)]
Center for Nanoscale Science and Technology, NIST, Gaithersburg, Maryland 20899

G. M. Rutter
School of Physics, Georgia Institute of Technology, Atlanta, Georgia 30332

J. N. Crain
Center for Nanoscale Science and Technology, NIST, Gaithersburg, Maryland 20899

C. Heiliger
Center for Nanoscale Science and Technology, NIST, Gaithersburg, Maryland 20899 and Maryland Nano Center, University of Maryland, College Park, Maryland 20742

P. N. First[b),c)]
School of Physics, Georgia Institute of Technology, Atlanta, Georgia 30332

J. A. Stroscio[b),d)]
Center for Nanoscale Science and Technology, NIST, Gaithersburg, Maryland 20899

(Received 8 October 2007; accepted 25 February 2008; published 1 July 2008)

The growth of graphene on the silicon-terminated face of 6*H*-SiC(0001) was investigated by scanning tunneling microscopy (STM) measurements. The initial stages of ultrahigh vacuum graphitization resulted in the growth of individual graphene sheets on random SiC terraces. These initial graphene sheets contained few defects, and the regions of clean SiC were free of contamination, exhibiting a $6\sqrt{3}\times 6\sqrt{3}R30°$ surface reconstruction. However, graphitization to multilayer thickness resulted in multiple defects, as observed with the STM. A high density of defects was observed, which may be attributed to the initial treatment of the SiC wafer. We characterize these defects, showing that they are located predominantly below the first layer of graphene. © *2008 American Vacuum Society.* [DOI: 10.1116/1.2900661]

I. INTRODUCTION

Over the past few years, there has been a tremendous growth in the experimental investigation of graphene, a two-dimensional honeycomb lattice of sp^2 bonded carbon atoms.[1] This unique material combines low dimensionality with high mobility, is a zero-gap semiconductor, and has a unique band structure resulting in charge carriers that can be thought of as massless Dirac fermions. These properties are appealing from both a technological point of view and for the study of fundamental quantum physics; the latter has been demonstrated by recent transport measurements through exfoliated and epitaxially grown graphene.[2–10] While exfoliated graphene is currently limited to few device fabrication and test bed applications, epitaxially grown graphene, in particular, on SiC,[11–13] has shown increasing promise for large-scale device fabrication.[14]

Early research revealed that thermal processing of SiC at elevated temperatures resulted in the layered growth of graphite on the surface.[15] This graphitization is due to the thermal decomposition of the SiC, where silicon evaporates from the surface and the remaining carbon atoms nucleate to form graphene sheets. Several early studies investigated the evolution of the SiC surface reconstruction up to and beyond the point of graphitization.[11–22] In fact, particular studies identified initial regions of graphite formation that appear to be single sheets of graphene.[11–13,17]

More recently, efforts have been made to utilize the thermal graphitization of SiC for the development of graphene-based devices.[2–4] This approach takes advantage of the fact that multilayered graphene forms uniformly over the SiC surface, thereby having the potential for large-scale device fabrication. Although many of the initial device structures consisted of multiple layers of graphene, measurements have resulted in unique transport properties that are inherent to graphene rather than bulk graphite. In spite of these promising results, graphitized SiC has yet to demonstrate a fully developed quantum Hall effect, as is seen in exfoliated graphene and conventional high-mobility two-dimensional electron systems. The growth of epitaxial graphene on SiC depends on many parameters, each of which may affect the quality of the graphene film and its transport properties. The effects of substrate preparation, growth procedures, multilayer material, and interaction between graphene and the SiC interface all must be understood in detail to realize the potential of this new electronic material.

In this article, a UHV scanning tunneling microscopy (STM) is utilized to characterize various defects that form during the UHV graphitization of the silicon-terminated face of 6*H*-SiC(0001). For SiC substrates prepared by hydrogen etching, the initial stages of graphitization have been imaged at the atomic scale and reveal an overall clean surface with

a)Electronic mail: nguisinger@anl.gov
b)Authors to whom correspondence should be addressed.
c)Electronic mail: joseph.stroscio@nist.gov
d)Electronic mail: first@physics.gatech.edu

regions of relatively defect-free graphene. On other, as-received samples, a significant number of defects are observed in the topographic STM images after multiple layers of graphene are grown. Although a systematic study of the defect density between pretreated hydrogen etched samples and as-received SiC substrates has yet to be carried out, the defect density is higher on the as-received samples than is typically found for hydrogen etched SiC. However, the reported defects are characteristic for both overlayer/substrate systems. Three distinct features have been imaged and appear to be the dominant defects in the graphene films. The observed defects are classified as sixfold scattering centers, randomly shaped ring structures, and "carbon nanotubes" (CNTs); although we are unable to determine whether complete cylinders are formed). Furthermore, the results of this study suggest that the observed defects are predominantly below the top layer of graphene close to the interface, and can potentially influence transport through these films.

II. EXPERIMENT

All experiments were performed at room temperature in a custom built UHV STM system. Electrochemically etched Ir STM probes were used throughout, following *in situ* annealing and field evaporation to clean the tip apex. The 6*H*-SiC(0001) was commercially purchased, doped *n* type. This study examined both treated and untreated 6*H*-SiC(0001) by an *ex situ* hydrogen etch. This etch removes deep scratches left by the commercial polishing of the wafer and consists of exposing the sample to an ambient pressure of hydrogen for 30 min at 1550 °C. Data from etched samples are shown in Fig. 1. Growth of multilayer graphene on the non-H etched sample showed a large number of defects, which are characterized in this study (Figs. 2–4).

The 6*H*-SiC(0001) samples were initially degreased with acetone and isopropyl alcohol followed by introduction into the UHV chamber, and degassed at 600 °C for at least 8 h. Heating was achieved resistively by passing current through the sample, which was held by molybdenum clips that also served as electrical contact. It should be noted that initial attempts at graphitization failed due to extended degassing above 600 °C, which resulted in large amorphous features on the surface. Following the sample degas, graphitization was performed by rapidly flashing the sample to the desired temperature. For initial stages of growth, each sample was flashed at 1200 °C for 30 s then cooled to room temperature a total of five times. For multilayered graphene, the flashing was conducted at 1250 °C for 2 min a total of five consecutive times. Following graphitization, the silicon-terminated face of the sample was characterized with the UHV STM without leaving vacuum.

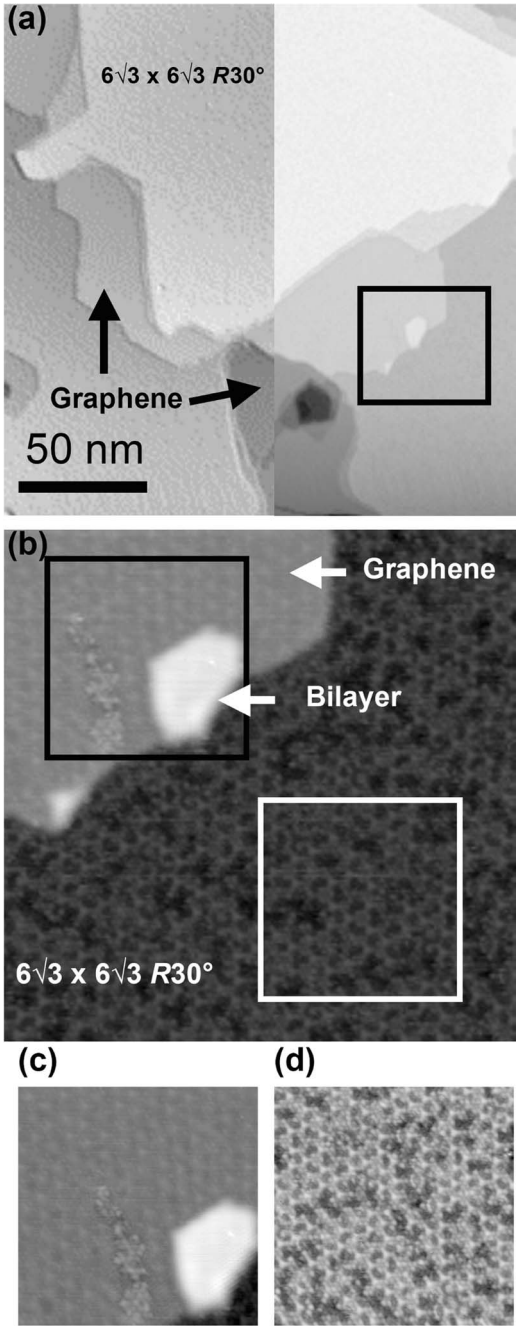

FIG. 1. (a) Large-scale STM image representative of a pretreated hydrogen etched surface following thermal processing at 1200 °C (imaging conditions: +1.0 V bias, 0.1 nA tunneling current). An enhanced gradient has been applied to the left hand portion of the image, in which the regions of graphene appear smoother than the clean SiC background. (b) STM image of the square inset in (a) clearly showing the transition from one layer of graphene to the $6\sqrt{3}\times 6\sqrt{3}R30°$ surface reconstruction of the clean SiC. [(c) and (d)] Closer views at the two respective regions.

III. RESULTS AND DISCUSSION

A. Initial stages of graphitization

The STM image of Fig. 1(a) is a large area scan representative of the SiC surface following 1200 °C thermal cycling in UHV. The majority of the surface is clean SiC with a $6\sqrt{3}\times 6\sqrt{3}R30°$ surface reconstruction. Although, the STM is unable to determine whether this surface reconstruction is silicon or carbon rich, topographic images clearly identify several terraces that show the initial growth of individual graphene sheets. These regions of graphene can be easily mistaken for clean SiC terraces. However, since the SiC re-

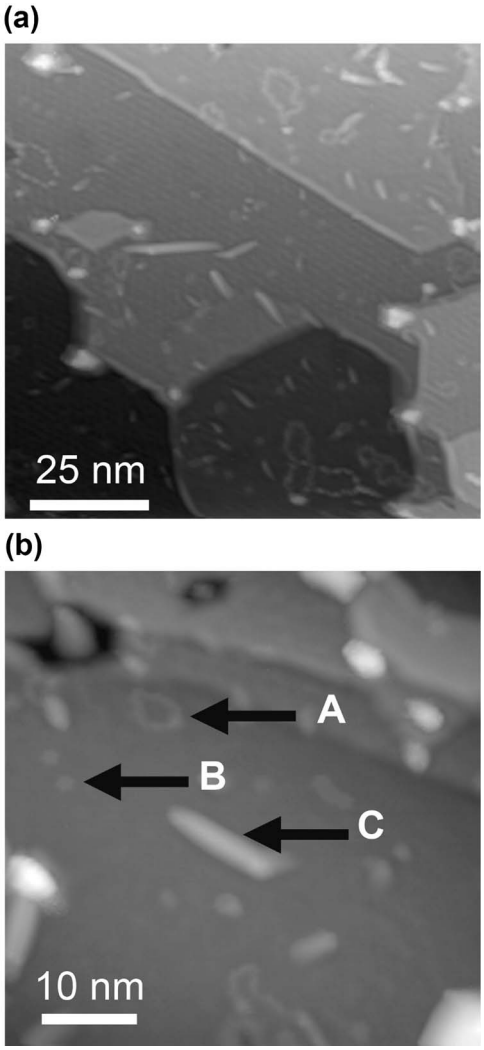

FIG. 2. (a) STM image of an as-received surface following multilayer growth of graphene on SiC at 1250 °C (imaging conditions: +1.0 V bias, 0.1 nA tunneling current). The image reveals a high concentration of defects within the graphene overlayer. (b) The three predominant defects are labeled A: ring structure defects, B: sixfold scattering defects, and C: CNTs growing parallel to the surface.

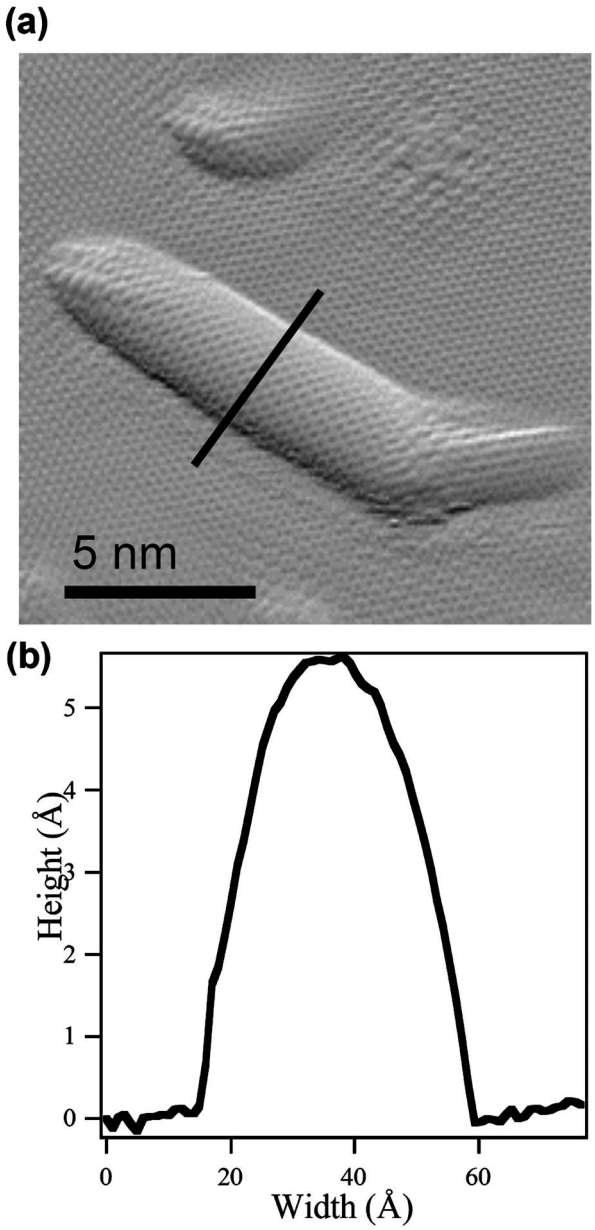

FIG. 3. (a) Enhanced gradient STM image resolving the as-received graphitized SiC surface, while focusing on an isolated CNT (imaging conditions: −0.2 V bias, 0.1 nA tunneling current). (b) Cross-sectional slice taken over the nanotube yielding a height of roughly 0.6 nm and a width of approximately 4.0 nm.

constructed surface is atomically rougher than graphene, they can be distinguished by applying a simple gradient enhancement to the image as shown in Fig. 1(a). Within the gradient enhanced portion of the image, the regions of graphene appear much smoother than the clean SiC.

Figure 1(b) shows a closer look at the transition between the graphene (upper left hand portion of the image) and the clean SiC surface (lower right hand portion of the image). At elevated sample bias, the graphene regions appear to be semitransparent and the underlying $6\sqrt{3}\times 6\sqrt{3}R30°$ surface reconstruction is observed, consistent with recent reports.[23] At the edge of the graphene sheet, there is a large island, illustrated in the zoom in of Fig. 1(c), which is the formation of a second layer of graphene. The underlying surface reconstruction is significantly reduced in the image of the bilayer region.[24] To the left of the island is an amorphous region that extends like a tail into the graphene sheet. This amorphous region is either below the graphene or is a region that has not fully graphitized. The STM image of Fig. 1(d) is a further zoom in of the clean SiC showing the $6\sqrt{3}\times 6\sqrt{3}R30°$ surface reconstruction that appears to be degraded by the thermal processing.

These images show that during the initial stages of growth, the graphene sheets are of high quality with very few defects, while the remaining SiC appears free of contamination. The edges of the graphene sheets appear to conserve the crystallographic directions of the SiC terraces, which may result from registry with the underlying surface reconstruction. In addition, the graphitization occurs on random ter-

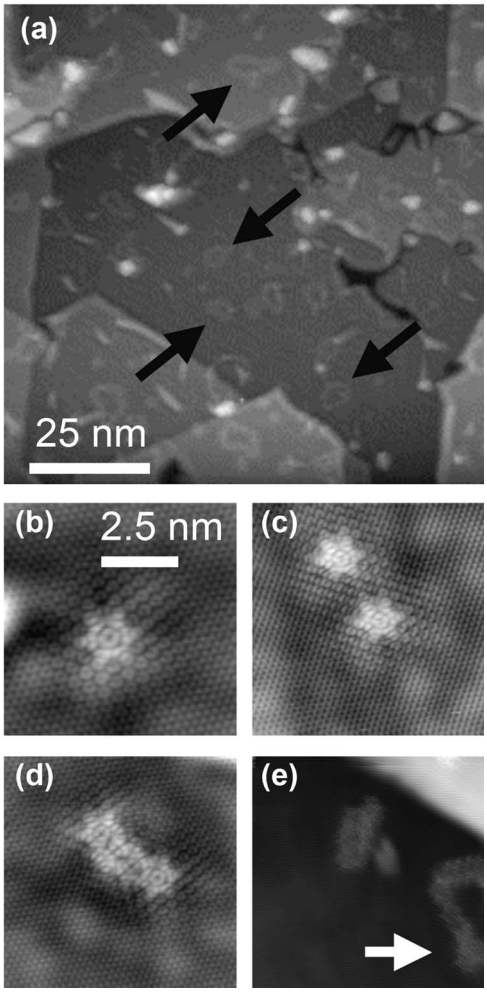

FIG. 4. (a) Large area STM image, of an as-received sample, showing several random ring structures on the surface, which have been highlighted with arrows (imaging conditions: +1.0 V bias, 0.1 nA tunneling current). [(b) and (c)] Isolated sixfold scattering defects. (d) Illustration that these defects are mobile at elevated temperature and tend to nucleate together (imaging conditions: +1.0 V bias, 0.1 nA tunneling current). (e) A short segment of nucleated sixfold scattering defects as well as a portion of a random ring structure, which also appears to be a nucleation of the scattering defects and is highlighted with an arrow.

races that are at different levels of the surface and not necessarily the topmost terrace, as illustrated in Fig. 1(a). This is surprising because further thermal processing to multilayer thickness, as discussed in the next section, appears to result in long range continuous sheets that blanket the surface.

B. Common defects in multilayer graphene

After characterizing the initial stage of graphitization, samples were processed at 1250 °C, resulting in multilayer graphene coverage. The STM image of Fig. 2(a) shows a large area scan of a fully graphitized surface. It is difficult to determine the actual thickness of the graphitized surface with the STM alone at this stage of growth. Underlying SiC terraces are clearly observed, while close inspection reveals that the graphene appears to be one continuous film over these steps. Unlike the initial stage of graphitization, this surface has an appreciable concentration of defects. Analysis of multiple samples over large surface areas reveals three predominant defects highlighted by arrows in Fig. 2(b). These defects are labeled (A) ring structure defects, (B) sixfold scattering defects, and (C) CNTs. The density of these defects is fairly constant over large areas, and we believe that the majority of these defects lie below the topmost layer of graphene.

The high resolution STM image of Fig. 3(a) shows a short CNT growing parallel to the surface, while the graphitized SiC can be clearly resolved in the background. The observed CNTs have been previously reported to grow parallel to the surface for silicon-terminated SiC and perpendicular to the surface for the carbon terminated face.[25–27] In fact, at higher processing temperatures, the CNTs form large networks that align to the atomic structure of the underlying SiC.[25]

An interesting question to answer is whether or not the observed CNTs are at the surface or are covered by graphene. To address this, we conducted scanning tunneling spectroscopy over the carbon nanotube and the graphitized background finding the spectra to be identical over both regions. A detailed examination of the atomic lattice in the vicinity of the CNT indicates that a layer of graphene is covering the CNT (i.e., the CNT is underneath the top graphene layer). In addition, the cross-sectional line scan of Fig. 3(b) indicates that the height of the tube is roughly 0.5 nm and the full width at half maximum is roughly 4.0 nm. A typical single-walled CNT has a diameter of roughly 1.0 nm. Therefore, if a layer of graphene is covering the CNT, it can compress the tube resulting in a reduced height and wider cross section as the graphene extends back to the surface.

Another defect, which has also been previously reported,[24,28] appears as a pointlike defect that exhibits sixfold scattering, as illustrated in the STM image of Figs. 4(a) and 4(b). This defect is always centered in the middle of a benzene ring in the topmost layer of graphene and has only been observed for graphitized SiC. We believe that this defect is either a carbon vacancy or a carbon atom that has been substituted by a silicon atom; both models are currently being theoretically explored with computational methods. We also believe that these defects lie below the topmost layer of graphene. Vacancies in the surface of graphite have been previously observed experimentally and numerous computational models have explored various defects at the surface,[29–41] all of which result in threefold scattering patterns due to the symmetry at a graphene lattice point. Therefore, a vacancy or a silicon atom within the graphene sheet should result in a threefold pattern in the topmost layer of graphene, which is not observed in the STM images for this defect. However, these graphene sheets follow a Bernal *AB AB* stacking and a lattice defect in the sheet directly below the top layer would be aligned to the center of a carbon ring in the topmost layer. This position does have sixfold symmetry and a projection from the underlying defect could result in the observed STM images.

The sixfold scattering defects also appear to be responsible for the numerous ring structures that are highlighted by arrows in the STM image of Fig. 4(a). These ring structures are both random in shape and size. Many rings extend over step edges and, in some cases, do not form closed loops. STM images reveal that these defects are mobile during the graphitization process and tend to nucleate together, as illustrated in Figs. 4(b)–4(d). A closer inspection of the ring structures suggests that these defects are the result of the sixfold scattering defects nucleating together, as highlighted in Fig. 4(e). These results support the hypothesis that the sixfold scattering sites are, in fact, lattice defects, and the nucleation into ring structures minimizes their perturbation of the lattice. Since the individual scattering defects are below the topmost layer of graphene, it is logical to assume that they also nucleate to form ring structures below the topmost layer of graphene.

IV. SUMMARY

We investigated the initial stages of graphene formation on the silicon-terminated face of 6*H*-SiC(0001) and characterized numerous defects observed after multilayer growth. The thermal processing of SiC at the initial stages of graphitization resulted in the growth of individual graphene sheets on random SiC terraces. The initial graphene sheets contained few defects and the overall surface was primarily free of contamination, and regions of clean SiC exhibited a $6\sqrt{3} \times 6\sqrt{3}R30°$ surface reconstruction. Graphitization of as-received SiC samples to multilayer graphene thickness resulted in a high density of atomic-scale defects.

The predominant defects observed with the STM are CNTs growing parallel to the surface, sixfold scattering defects, and ring structures that appear to be the nucleation of the scattering defects. This study suggests that all of the defects are located below the topmost graphene layer, which is a reasonable assessment when considering the graphene growth mechanisms by SiC decomposition. Unlike traditional epitaxial growth, in which material is added to a substrate, the graphitization of SiC involves the decomposition of the surface and loss of material. This "reverse" epitaxy results in the topmost graphene layer being the first to form, while the layer closest to the SiC interface is the last. Once the surface is capped with the first layer of graphene, mass transfer (i.e., carbon nucleation and silicon evaporation) is impeded and can thereby lead to defects during the formation of subsequent graphene layers. Therefore, consistent with the initial stages of growth, the topmost layer of graphene appears to be of the highest quality, while subsequent layers close to the interface appear to contain a higher density of defects. The overall quality of the starting surface may be important and result in a different defect density depending on hydrogen termination of the sample after hydrogen etching. Defects and contamination present during the graphitization may also play a roll. The observed defects can potentially affect transport through lower-lying graphene layers close to the interface.

ACKNOWLEDGMENTS

This work was supported in part by the NIST-CNST/UMD-NanoCenter Cooperative Agreement, by the Office of Naval Research, and by NSF Grant Nos. ECS-0404084 and ECS-0521041. One of the authors (N.P.G.) acknowledges a National Research Council Postdoctoral Fellowship. The authors also thank Mark Stiles for valuable comments and discussions, and Mike Sprinkle, Steven Blankenship, Frank Hess, and Alan Band for their technical assistance.

[1] A. K. Geim and K. S. Novoselov, Nat. Mater. **6**, 183 (2007).
[2] C. Berger *et al.*, J. Phys. Chem. B **108**, 19912 (2004).
[3] C. Berger *et al.*, Science **312**, 1191 (2006).
[4] W. A. de Heer *et al.*, Solid State Commun. **143**, 92 (2007).
[5] K. S. Novoselov *et al.*, Science **315**, 1379 (2007).
[6] Y. Zhang *et al.*, Phys. Rev. Lett. **96**, 136806 (2006).
[7] K. S. Novoselov, A. K. Geim, S. V. Morozov, D. Jiang, M. I. Katsnelson, I. V. Grigorieva, S. V. Dubonos, and A. A. Firsov, Nature (London) **438**, 197 (2005).
[8] Y. B. Zhang, Y. W. Tan, H. L. Stormer, and P. Kim, Nature (London) **438**, 201 (2005).
[9] K. S. Novoselov, D. Jiang, F. Schedin, T. J. Booth, V. V. Khotkevich, S. V. Morozov, and A. K. Geim, Proc. Natl. Acad. Sci. U.S.A. **102**, 10451 (2005).
[10] K. S. Novoselov, A. K. Geim, S. V. Morozov, D. Jiang, Y. Zhang, S. V. Dubonos, I. V. Grigorieva, and A. A. Firsov, Science **306**, 666 (2004).
[11] P. Martensson, F. Owman, and L. I. Johansson, Phys. Status Solidi B **202**, 501 (1997).
[12] F. Owman and P. Martensson, Surf. Sci. **330**, L639 (1995).
[13] F. Owman and P. Martensson, J. Vac. Sci. Technol. B **14**, 933 (1996).
[14] J. Kedzierski, P. Hsu, P. Healey, P. Wyatt, C. Keast, M. Sprinkle, C. Berger, and W. de Heer, e-print arXiv.cond-mat/0801.2744.
[15] A. J. Vanbommel, J. E. Crombeen, and A. Vantooren, Surf. Sci. **48**, 463 (1975).
[16] C. S. Chang, I. S. T. Tsong, Y. C. Wang, and R. F. Davis, Surf. Sci. **256**, 354 (1991).
[17] A. Charrier *et al.*, J. Appl. Phys. **92**, 2479 (2002).
[18] Y. Hisada, K. Hayashi, K. Kato, T. Aoyama, S. Mukainakano, and A. Ichimiya, Jpn. J. Appl. Phys., Part 1 **40**, 2211 (2001).
[19] M. A. Kulakov, P. Heuell, V. F. Tsvetkov, and B. Bullemer, Surf. Sci. **315**, 248 (1994).
[20] W. J. Ong, E. S. Tok, H. Xu, and A. T. S. Wee, Appl. Phys. Lett. **80**, 3406 (2002).
[21] E. S. Tok, W. J. Ong, and A. T. S. Wee, Surf. Sci. **558**, 145 (2004).
[22] M. H. Tsai, C. S. Chang, J. D. Dow, and I. S. T. Tsong, Phys. Rev. B **45**, 1327 (1992).
[23] G. M. Rutter, N. P. Guisinger, J. N. Crain, E. A. A. Jarvis, M. D. Stiles, T. Li, P. N. First, and J. A. Stroscio, Phys. Rev. B **76**, 235416 (2007).
[24] G. M. Rutter, J. N. Crain, N. P. Guisinger, T. Li, P. N. First, and J. A. Stroscio, Science **317**, 219 (2007).
[25] V. Derycke, R. Martel, M. Radosvljevic, F. M. R. Ross, and P. Avouris, Nano Lett. **2**, 1043 (2002).
[26] H. Watanabe, Y. Hisada, S. Mukainakano, and N. Tanaka, J. Microsc. **203**, 40 (2001).
[27] M. Kusunoki, T. Suzuki, T. Hirayama, N. Shibata, and K. Kaneko, Appl. Phys. Lett. **77**, 531 (2000).
[28] B. An, S. Fukuyama, and K. Yokogawa, Jpn. J. Appl. Phys., Part 1 **41**, 4890 (2002).
[29] Y. Ferro, C. Thomas, T. Angot, P. Genesio, and A. Allouche, J. Nucl. Mater. **363**, 1206 (2007).
[30] Y. Ferro and A. Allouche, Phys. Rev. B **75**, 155438 (2007).
[31] T. O. Wehling, A. V. Balatsky, M. I. Katsnelson, A. I. Lichtenstein, K. Scharnberg, and R. Wiesendanger, Phys. Rev. B **75**, 125425 (2007).
[32] Y. Niimi, H. Kambara, T. Matsui, D. Yoshioka, and H. Fukuyama, Phys. Rev. Lett. **97**, 236804 (2006).
[33] Z. F. Wang, R. X. Xiang, Q. W. Shi, J. L. Yang, X. P. Wang, J. G. Hou, and J. Chen, Phys. Rev. B **74**, 125417 (2006).
[34] P. Ruffieux, M. Melle-Franco, O. Groning, M. Bielmann, F. Zerbetto, and P. Groning, Phys. Rev. B **71**, 153403 (2005).

[35]A. Hashimoto, K. Suenaga, A. Gloter, K. Urita, and S. Iijima, Nature (London) **430**, 870 (2004).
[36]A. A. El-Barbary, R. H. Telling, C. P. Ewels, M. I. Heggie, and P. R. Briddon, Phys. Rev. B **68**, 144107 (2003).
[37]K. F. Kelly, E. T. Mickelson, R. H. Hauge, J. L. Margrave, and N. J. Halas, Proc. Natl. Acad. Sci. U.S.A. **97**, 10318 (2000).
[38]M. Kusunoki, T. Suzuki, T. Hirayama, N. Shibata, and K. Kaneko, Appl. Phys. Lett. **77**, 531 (2000).
[39]J. R. Hahn and H. Kang, Phys. Rev. B **60**, 6007 (1999).
[40]J. G. Kushmerick, K. F. Kelly, H. P. Rust, N. J. Halas, and P. S. Weiss, J. Phys. Chem. B **103**, 1619 (1999).
[41]K. F. Kelly, D. Sarkar, G. D. Hale, S. J. Oldenburg, and N. J. Halas, Science **273**, 1371 (1996).